


Article

Alkali and Alkaline Earth Metals (K, Ca, Sr) Promoted Cu/SiO₂ Catalyst for Hydrogenation of Methyl Acetate to Ethanol

Muhammad Naeem Younis ^{1,2,3,†} , Zhiheng Ren ^{2,†}, Chunshan Li ^{2,3}, Erqiang Wang ^{3,*} and Jie Li ^{1,2,*}

¹ Advanced Energy Science and Technology Guangdong Laboratory, Huizhou 516003, China

² Beijing Key Laboratory of Ionic Liquids Clean Process, Key Laboratory of Green Process and Engineering, Key Laboratory of Multiphase Complex Systems, Institute of Process Engineering, Chinese Academy of Sciences, Beijing 100190, China

³ School of Chemical Engineering, University of Chinese Academy of Sciences, Beijing 100049, China

* Correspondence: wangerqiang@ucas.ac.cn (E.W.); lijiequst@ipe.ac.cn (J.L.)

† These authors contributed equally to this work.

Abstract: The advancing effects of various alkali and alkaline earth metals (inclusive of K, Ca, and Sr) modified Cu/SiO₂ catalysts, prepared with a modified precipitation-gel method, were investigated for the production of ethanol via hydrogenation of methyl acetate. Our results showed that Sr-doped catalysts exhibited the best and most consistent results during catalytic tests. A series of techniques, including X-ray diffraction technique, Raman spectroscopy, N₂ adsorption/desorption, N₂O titration method, FTIR spectroscopy, and H₂ temperature, programmed desorption and reduction (TPD and TPR), and X-ray Photoelectron Spectroscopy, which was used to check the detailed characterization of Sr modification in the catalyst and its structural impacts on the properties of the catalyst. These results demonstrated that the addition of 5%Sr could strengthen the intrinsic stability of the catalyst by formulating the appropriate ratio of Cu⁺/(Cu⁰ + Cu⁺) to facilitate catalytic outcome improvement. The addition of 5%Sr-30%Cu/SiO₂ under the most favorable conditions, resulting in the peak conversion of MA (95%) and ethanol selectivity (96%), indicates its magnificent catalytic stabilizing effects. Furthermore, the best performing catalyst was compared and tested under various conditions (LHSV and temperatures) and a 300 h long life run.

Keywords: hydrogenation; methyl acetate; ethanol; strontium



Citation: Younis, M.N.; Ren, Z.; Li, C.; Wang, E.; Li, J. Alkali and Alkaline Earth Metals (K, Ca, Sr) Promoted Cu/SiO₂ Catalyst for Hydrogenation of Methyl Acetate to Ethanol. *Catalysts* **2023**, *13*, 450. <https://doi.org/10.3390/catal13020450>

Academic Editor: Kevin J. Smith

Received: 28 December 2022

Revised: 11 February 2023

Accepted: 16 February 2023

Published: 20 February 2023



Copyright: © 2023 by the authors. Licensee MDPI, Basel, Switzerland. This article is an open access article distributed under the terms and conditions of the Creative Commons Attribution (CC BY) license (<https://creativecommons.org/licenses/by/4.0/>).

1. Introduction

Ethanol possesses an eco-friendly nature and acts as a renewable biofuel and sustainable energy source. It has been produced by using various biomass fermenting techniques for a long time, via different biological steps, all with high cost [1,2]. In this advanced research era, a new catalytic hydrogenation method to synthesize ethanol has gained remarkable attention, as the equipment used for the whole preparatory phase is economical, simple, and efficient as compared to expensive equipment used in acetic acid hydrogenation [3,4]. The hydrogenation of methyl acetate (MA) to synthesize ethanol is getting remarkable attention, as the MA being used is obtained from reacting acetic acid with methanol, which may further cut down the excessiveness of acetic acid and prevent its hydrogenation shortcomings [5]. Another source of MA is natural gas and coal, which is the result of a recent outpour towards the usage of shale gas and coal. Therefore, the hydrogenation of MA could be an economical and environment friendly process [6].

Various preparatory techniques have been used to formulate highly efficient catalysts in the hydrogenation process, including ammonia evaporation procedure [7–10], ion exchange method [11], impregnation technique [12], and urea precipitation method [13,14]. In MA hydrogenation, Cu/SiO₂ is the preferred catalyst because of its irreducible SiO₂ support and economical characteristics [15–17], and it constitutes sufficient Cu to improve the efficiency of the overall procedure [9]. According to previous literature, a Cu-based

catalyst was found to be very active for C=O bond hydrogenation but inactive for C-C bond cleavage, although many of the precious metal catalysts behave otherwise [18–24]. Cu^+ sites concentration on the surface of the catalyst supported strong bonding and adsorption of methoxy and acyl groups, while Cu^0 sites supported hydrogen decomposition [25]. It has been demonstrated that the coexistence, balancing, appropriate distribution, and cooperated association between both Cu^0 and Cu^+ sites synergistically presented an enhanced catalytic effect and stability [5].

Cu/SiO₂ catalyst modification with chromium (Cr) oxide has been a favored catalyst due to its greater stability and catalytic activity, but Cr toxicity causing ecological issues has made its applicability very restricted [26,27]. Instead of Cr, the catalytic performance of Cu/SiO₂ could also be enhanced, stabilized, and made efficient by adding one more metal like Ce, La, Mg, Ag, Zn, Mn, In, B, or Ni, specifically increasing the concentration of Cu^+ on the surface area and Cu dispersion [6,22,28–36]. The role of metal oxides in addition to the catalyst has been found to give signifying results owing to their agglomerating and sintering characteristics. A positive response of Zn-modified Cu/SiO₂ catalyst was reported by Ying Ming et al. as demonstrating excellent activity of the catalyst for ethanol synthesis through ethyl acetate hydrogenation [37]. La-oxide addition to Cu/SiO₂ to generate ethylene glycol via dimethyl oxalate hydrogenation was found to be significant to promote the activity of the catalyst [38]. CeO₂-loaded Cu/SiO₂ was examined by Ye et al., showing promoted results of the catalyst and stability via the reduction of Cu crystals and its dispersion enhancement [8].

It has been reported that promotion with alkali and alkaline metals of the catalyst Cu/SiO₂ could generate the basic sites and influence the electronic structure of metal particles, which enhances the thermic stability and surface Cu dispersion during overall hydrogenation [39]. The addition of alkali earth metals could influence the active metal particles by stabilizing the small size of active metals and ultimately reducing the chances of agglomeration [40,41]. It was also reported that the addition of Ca, Sr, and K could increase surface area and enhance catalytic activity [42,43]. The structural composition of the catalyst, high Cu dispersion at the surface, strong Cu and silica chemical bonding, surface modifications, and the appropriate surface ratio of $\text{Cu}^+ / (\text{Cu}^0 + \text{Cu}^+)$ all are vital characteristics for the promotion of catalytic efficiency. However, Cu catalysts are still challenging to overcome in their short lifetime, and the copper-silica interactions and the variations in structural composition during the whole hydrogenation procedure were hardly investigated. As far as we know, no detailed study has been reported on K, Ca, and Sr-modified Cu/SiO₂ catalyst systems prepared by using the precipitation gel method for the hydrogenation reaction of MA.

In the present research work, the promoting effects of alkali and alkaline earth metals (K, Ca, and Sr) modified Cu/SiO₂ catalysts for MA hydrogenation to produce ethanol was examined. The modified precipitation gel method was used to prepare the series of catalysts, and various analytical techniques were used to check the characterization of the prepared catalyst for the evaluation of promotor and copper interactions. By modifying additive quantities of Sr in the catalyst, the suitable ratio was finalized for Cu/SiO₂ for MA hydrogenation to synthesize ethanol over 5%Sr-30%Cu/SiO₂.

2. Results and Discussion

2.1. Physicochemical Properties of the Catalysts

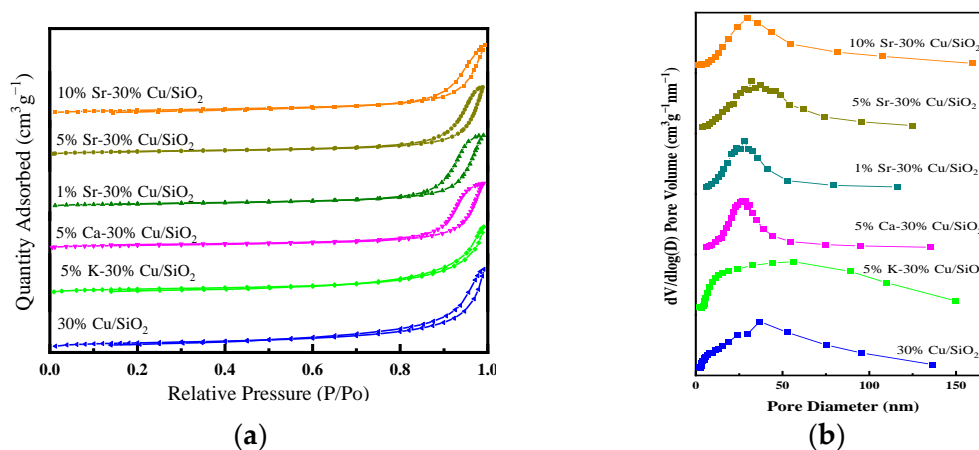
The chemical compositions of the catalysts were estimated by ICP-AES and presented in Table 1, and these values were slightly lower than the designed values because some metal ions were weakly absorbed on silica gel and eluted during the repeated washing process.

Table 1. Structural properties of xM-30%Cu/SiO₂ catalyst.

Catalyst	Content ^a		S _{BET} ^b (m ² /g)	BJHV _p ^b (cm ³ /g)	BJHD _p ^b (nm)	S _{Cu} ^{0 c} (m ² /g)	S _{Cu} ^{+ d} (m ² /g)	S _{Cu} (m ² /g)
	Cu	M						
30%Cu/SiO ₂	30.2	–	50.0	0.19	16.8	33.7	31.2	64.9
5%K-30%Cu/SiO ₂	26.6	4.6	50.2	0.20	19.0	34.9	37.8	72.7
5%Ca-30%Cu/SiO ₂	27.1	4.4	114.8	0.73	23.9	35.4	34.2	69.6
1%Sr-30%Cu/SiO ₂	28.3	0.92	79.9	0.52	23.4	36.1	38.6	74.7
5%Sr-30%Cu/SiO ₂	26.8	4.5	119.3	0.76	26.8	36.2	44.6	80.8
10%Sr-30%Cu/SiO ₂	25.9	8.7	41.4	0.25	21.5	34.5	38.6	73.1
AS-40 SiO ₂	–	–	129–155		20–24			

^a Obtained by ICP-OES. ^b Obtained from N₂ adsorption isotherm. ^{c,d} Calculated S_{Cu} by N₂O titration and S_{Cu}⁺ by LMM XAES spectra combined with N₂O titration.

The BET analysis was conducted to get the N₂ adsorption–desorption isotherms and the BJH (Barret–Joyner–Halenda) pore size distribution of these catalysts, as exhibited in Figure 1. The isotherms of all the catalysts have followed the IUPAC type IV isotherms pattern, where a hysteresis loop was formed from $p/p^0 \approx 0.6$ –1.0, indicating the existence of a typical H3 class mesoporous structure [7,44]. The surface area (BET), and mean pore diameter (BJH method) of the support and catalysts are tabulated in Table 1, which indicates that the BET surface significantly improved in the promoted catalyst, with 5% Sr-promoted catalyst showing the maximum surface area of 119.3 m²/g. It is also of substantial importance that the BJH-pore volume of promoted catalysts also increased, which is a reason for improved activity and stability. Although the addition of promotor enhances the copper dispersion and decreases the aggregation of copper species, which usually causes the obstruction of pores, we observed increased BET surface area, pore diameter, and pore volume in the case of 5%Sr-30%Cu/SiO₂ catalyst, as explained in TEM and XPS analysis in Sections 3.3 and 3.5, respectively. However, the results also indicated that when the loading of Sr was further increased, BET surface area and BJH-pore volume decreased, which also explains the reduced MA conversion and selectivity of ethanol due to the formation of agglomerates [28,39]. Figure 1 revealed that the pore size of promoted catalysts lies in the range of 10–60 nm in most of the promoted catalysts.

**Figure 1.** Calcined xM-30%Cu/SiO₂ catalysts. (a) N₂ adsorption–desorption isotherm and (b) BJH pore size distribution curves.

In addition, copper species distribution during the hydrogenation of MA is crucial in determining the catalytic activities of Cu-based catalysts; therefore, the copper surface area of reduced catalysts was estimated via N₂O titration and combined with CO-TPD and XAES analysis [29]. Following the introduction of the promoter, the surface area of Cu⁺ is increased in the reduced sample, whereas the surface area of Cu⁰ does not differ much from Cu/SiO₂, as shown in Table 1. Cu/SiO₂ with increased Sr content exhibits higher

S_{Cu+} values than other catalysts, and 5%Sr-30%Cu/SiO₂, in particular, displays the highest S_{Cu+} (44.6 m²/g). Nevertheless, a sufficient amount of Sr may increase S_{Cu+} values without adverse consequences, which might be caused by the coating of strontium oxide on the catalyst surface.

2.2. Crystalline Phase and Morphology

XRD patterns of all the calcined and freshly reduced catalysts are presented in Figure 2a,b, respectively. A diffuse and broad diffraction peak at 21.8° was observed in all XRD patterns that could be assigned to amorphous silica [7]. In all of the calcined catalysts, diffraction peaks related to CuO were observed at 35.5° and 38.7° (JCPDS 05-0661). The diffraction peaks for CuO in promoted catalysts were much broader and less intense as compared to non-promoted catalysts. However, these peaks disappeared in reduced patterns shown in Figure 2b. Metallic Cu peaks at 43° and 50° (JCPDS 04-0836) were observed, and the phase attributed to Cu₂O was noted at 36.5° (JCPDS 05-0667) in all promoted catalysts [7,45]. Table 2 listed the particle size of Cu (111) in all the freshly reduced studied catalysts, and it was revealed that the particle size of Cu metal was larger in non-promoted catalysts as compared to promoted catalysts. However, no visible diffraction peaks of promoted metals (K, Ca, or Sr) or their oxides were observed in the XRD patterns, hence, it could be established that these metal oxides were highly dispersed in these catalysts. It is also evident from Table 2 that in the case of Ca and Sr, Cu(111) particle size reduced as compared to non-promoted catalysts significantly. It was also observed that non-promoted catalyst Cu⁰ contents were very high as compared to Cu²⁺-contents, which is also in accordance with the studies of Wang et al. However, with the introduction of promoted metal, a broader peak of Cu₂O could easily be observed with a less intense peak of Cu⁰ [46].

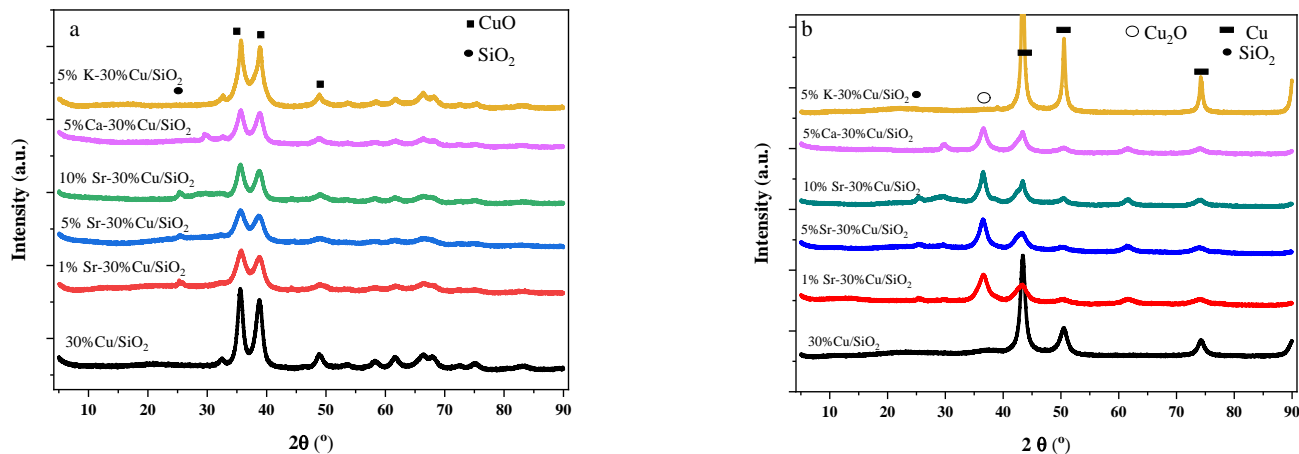


Figure 2. XRD patterns of (a) calcined and (b) reduced Cu/SiO₂ and xM-30%Cu/SiO₂ catalysts.

Table 2. Particle sizes of metallic Cu (111) of all promoted and non-promoted catalysts.

Catalyst	2θ of Cu (111)	d _{Cu} (nm)	d _{Cu2+} (nm)
30%Cu/SiO ₂	43.4	4.8	4.4
5%K-30% Cu/SiO ₂	43.4	9.5	4.3
5%Ca-30% Cu/SiO ₂	43.2	4.6	5.3
1%Sr-30% Cu/SiO ₂	43.1	3.7	4.0
5%Sr-30% Cu/SiO ₂	43.0	4.0	4.8
10%Sr-30% Cu/SiO ₂	43.2	4.9	6.2

The absorption peaks of FTIR spectra shown in Figure 3 confirmed the presence of Cu phyllosilicate in promoted and non-promoted catalysts, and this fact could be supported by the appearance of the δ_{OH} band at 670 cm^{−1} and the ν_{SiO} shoulder peak at 1040 cm^{−1} [47].

The weak band observed at 670 cm^{-1} could be ascribed to δ_{OH} bond of $\text{Cu}_2\text{SiO}_5(\text{OH})_2$ [48]. All the promoted catalysts were initially dried and at that stage $\text{Cu}_2\text{SiO}_5(\text{OH})_2$ structure was formed, but during the calcination stage this structure vanishes, hence, very faint peaks were observed in FTIR. However, strong diffraction peaks related to CuO were observed at 35.5° and 38.7° in XRD patterns, due to which minor peaks related to $\text{Cu}_2\text{SiO}_5(\text{OH})_2$ might have covered, which also suggests its maximum decomposition after calcination [10]. Furthermore, the presence of band at 670 cm^{-1} related to copper phyllosilicate could be observed in all the promoted and nonpromoted catalysts, referring to the fact that this structure is largely preserved in all catalysts, however, its intensity varies in different catalysts, with 5%K-30%Cu/SiO₂ showing the strongest intensity of the peak. The band observed at 490 cm^{-1} in all of the promoted and non-promoted catalysts may be due to CuO stretching vibrations [49,50]. Accordingly, the bands observed at 1110 cm^{-1} , 800 cm^{-1} , and 490 cm^{-1} could be attributed to the existence of SiO₂ and copper oxides in the catalysts, which is also in agreement with XRD results.

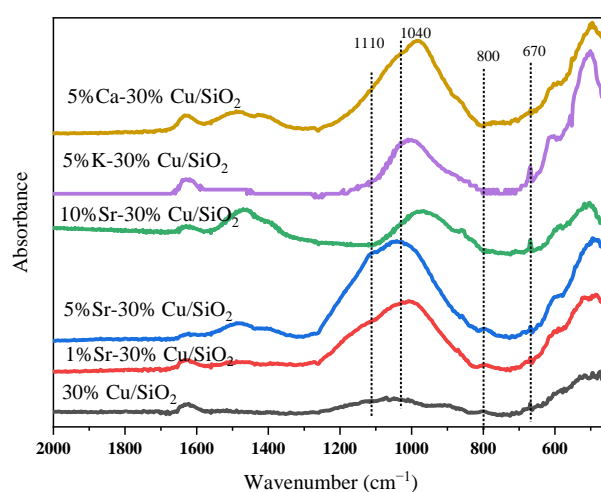


Figure 3. FTIR spectra of calcined Cu/SiO₂ and xM-30%Cu/SiO₂ catalysts.

Figure 4 represents the TEM images and average Cu particle size distribution of best-performing 5%Sr-30%Cu/SiO₂ and representative Cu/SiO₂ catalysts to better understand the morphology of the catalyst series. The high dispersion state of Cu and Sr in 5%Sr-30%Cu/SiO₂ catalyst was confirmed by TEM analysis, as shown in Figure 4a. The high-resolution transmission electron microscope image of Cu (111) nanocrystals revealed a clear crystal face structure with a lattice spacing of ca. 0.208 nm. Various diffraction rings and spots were seen in its selected area of electron diffraction (SAED). The reduced samples of Figure 4a,c show that the metallic black copper species are dispersed well on the silica, and the mean sizes for 5%Sr-30%Cu/SiO₂ and Cu/SiO₂ are 3.43 nm and 4.71 nm, respectively, suggesting that promotion with Sr makes the particles less prone to agglomeration. The TEM images in Figure 4g and respective particle size distribution in Figure 4h give more insight into the reason of 30%Cu/SiO₂ deactivation after long-term testing of 300 h, where mean particle size increases from 4.71 nm to 7.07 nm. However, Figure 4e,f further show that the probable reason of better performance shown by 5%Sr-30%Cu/SiO₂ among other catalysts might be its thermal stability, enhanced dispersion, and resistance towards copper aggregation and coagulation even after 300 h and minor increases in mean particle size of 5.38 nm, respectively. In addition, FESEM image of elemental mapping of reduced 5%Sr-30%Cu/SiO₂ catalyst and the corresponding EDS elemental mappings of Cu and Sr (Figure 4i) suggest that both species are co-existent and uniformly dispersed on the silica texture.

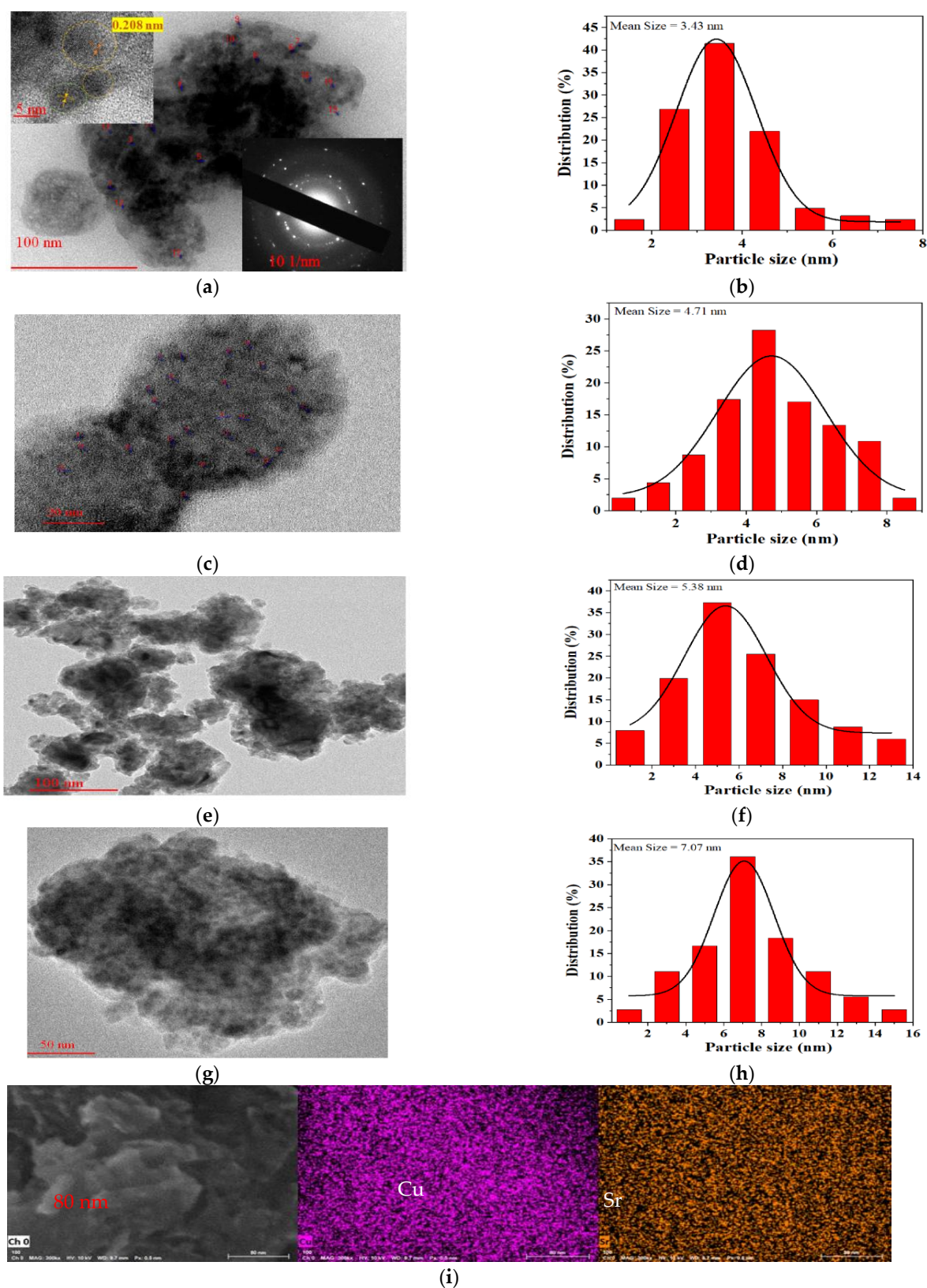


Figure 4. (a,c) TEM images of freshly reduced 5%Sr-30%Cu/SiO₂ and 30%Cu/SiO₂ catalyst, and (b,d) represent the particle size distribution, respectively; (e,g) TEM images of spent 5%Sr-30%Cu/SiO₂ and 30%Cu/SiO₂ catalyst; (f,h) are respective size distribution; (i) FESEM image of elemental map of reduced 5%Sr-30%Cu/SiO₂ catalyst and the corresponding EDS elemental mappings of Cu and Sr.

2.3. H_2 -TPR and H_2 -TPD

The H_2 -TPR experiments were conducted, and profiles were recorded to investigate the reducibility of previously calcined Cu/SiO₂ and xM-30%Cu/SiO₂ catalysts. Figure 5 shows that the reduction peak centered at 201 °C of Cu/SiO₂ catalyst, which results from the reduction of well-dispersed CuO and copper phyllosilicate [28]. According to the literature, the first peak is usually ascribed to well-dispersed CuO, and it appears at 191 °C in 30%Cu/SiO₂ and at 186 °C in 5%K-30%Cu/SiO₂. However, in the rest of the promoted catalysts, both low temperature peaks are merged and can be seen in Figure 5 [51]. Furthermore, observing the enlarged profiles revealed a third broader reduction peak that starts after 250 °C. This peak is easily identifiable in 30%Cu/SiO₂ and is associated with the reduction of larger CuO crystallites and the partial reduction of Cu²⁺ to Cu⁺ as a result of higher copper loading (30%), which is consistent with XRD results. However, in the 5%Sr-30%Cu/SiO₂ catalyst, this broader reduction peak is most likely caused by interactions between Cu species and Sr, since there is no obvious evidence to suggest the existence of large CuO crystallites from TPR profiles, which agrees with the XRD patterns.

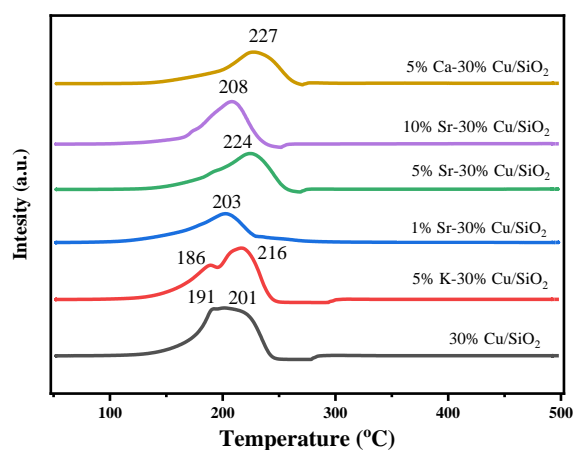


Figure 5. H_2 -TPR profiles of 30%Cu/SiO₂ and xM-30%Cu/SiO₂ catalysts.

Figure 6 shows the TPD profiles of hydrogen desorption from Cu/SiO₂ and promoted catalysts. H_2 -TPD is a dynamic method that was used to analyze the adsorption behavior of H_2 on preactivated (in pure hydrogen) catalysts. Two significant desorption peaks have been observed in all catalysts. The first, ranging from 50 °C to 130 °C, is linked to the chemisorbed H_2 on the surface of the Cu, and the second broader peak ranges from 135 °C to 450 °C, which could be related to the chemisorbed splitting H species on the surface of the catalyst [52,53]. Moreover, the presence of a broader peak could be an indicator of many small metal particles [54]. In addition, the amount of H_2 desorption based on the second peak was calculated and was in the following order: 5%Sr-30%Cu/SiO₂ > 1%Sr-30%Cu/SiO₂ > 10%Sr-30%Cu/SiO₂ > 5%Ca-30%Cu/SiO₂ > 5%K-30%Cu/SiO₂ > 30%Cu/SiO₂. Among all tested catalysts, the adsorption of split H-H on 5%Sr-30%Cu/SiO₂ is the largest and that of 30%Cu/SiO₂ is the smallest, which is consistent with the catalytic activity, indicating the importance of split H-H adsorptions [55]. It is also clear from Figure 6 that the intensities of H_2 desorption peaks, as well as the amount of H_2 desorbed, are clearly affected by Sr loading because Cu loading was unchanged. Accordingly, the higher S_{Cu} value of 5%Sr-30%Cu/SiO₂, as shown in Table 1, and the intensities of broad high temperature peaks are enhanced by the promoter, suggesting that the presence of two chemisorbed H-species is linked to the introduction of the promoter in Cu/SiO₂-based catalysts. Hence, the Sr-promoted catalyst has significantly enhanced hydrogen activation by influencing the electronic structure of metal contents and their mobility on the support and the concentration of active H-species on the catalyst surface.

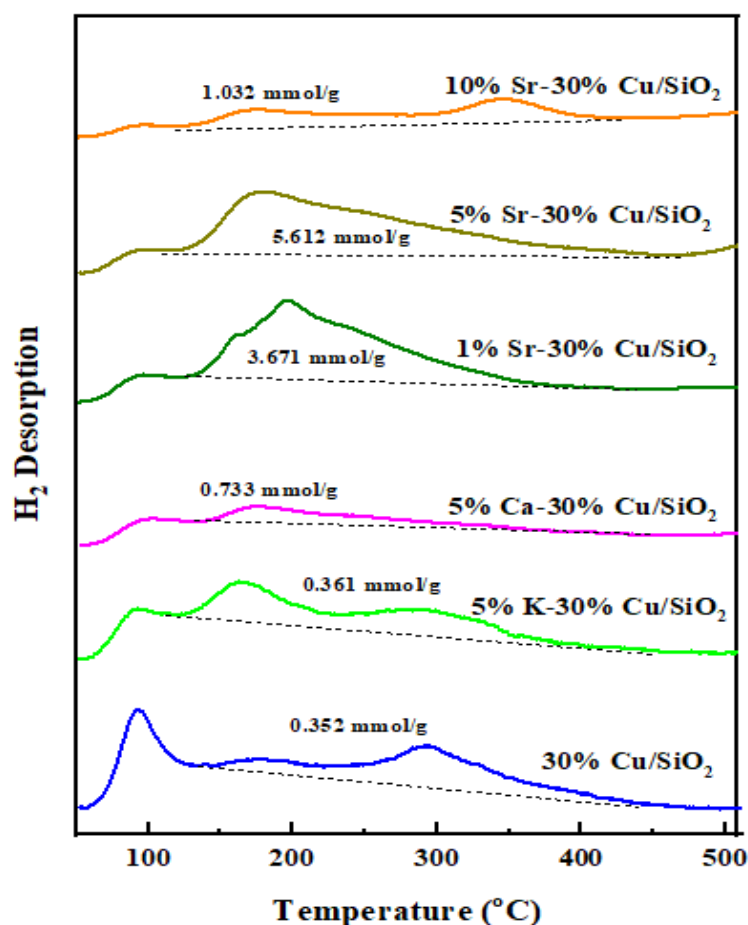


Figure 6. H₂-TPD profiles of reduced Cu/SiO₂ and xM-30%Cu/SiO₂ catalysts.

2.4. Chemical States of Surface Species

Figure 7a represents the XPS spectra and X-ray-induced Auger electron spectroscopy (XAES) of reduced samples of all promoted and non-promoted catalysts. As shown in the figure, two peaks associated with the Cu 2p_{1/2} and Cu 2p_{3/2} were observed at 952.02 and 932.19, respectively. Moreover, the absence of satellite peaks also suggests that Cu²⁺ species had been reduced into Cu⁰ or Cu⁺ species [56]. Since Cu⁰ and Cu⁺ have nearly identical binding energies, the Cu LMM XAES spectrum of reduced catalysts was recorded to determine the amounts of surface Cu⁺ and Cu⁰ species [57]. According to Figure 7b, Sr exists only as a divalent oxidation state of Sr 3d_{3/2} and Sr 3d_{5/2} in all Sr-promoted Cu/SiO₂ catalysts, as indicated by the two peaks at 133.7 and 135.3 eV, respectively, of the Sr 3d XPS curve. A slight shift in Sr 3d binding energies was also observed once Sr content was increased in the catalysts, which could be due to the build-up of strontium oxide species at the surface of the catalyst. The Cu⁺/(Cu⁰ + Cu⁺) ratio reached a maximum value of 0.6 when Cu/SiO₂ was promoted with 5 wt.% strontium, however, this ratio reduced to 0.54 when the amount of promoter increased to 10%, and this observation is consistent with XRD and H₂-TPR results. Zhang et al. had reported that the ratio of copper species on the surface of the catalyst could be affected by the alkaline nature of promoter. Thus, we speculated that in the case of 5%Ca-30%Cu/SiO₂, the decline in Cu⁺/(Cu⁰ + Cu⁺) ratio could be the reason for the mild alkaline nature of Ca metal as compared to Sr [45].

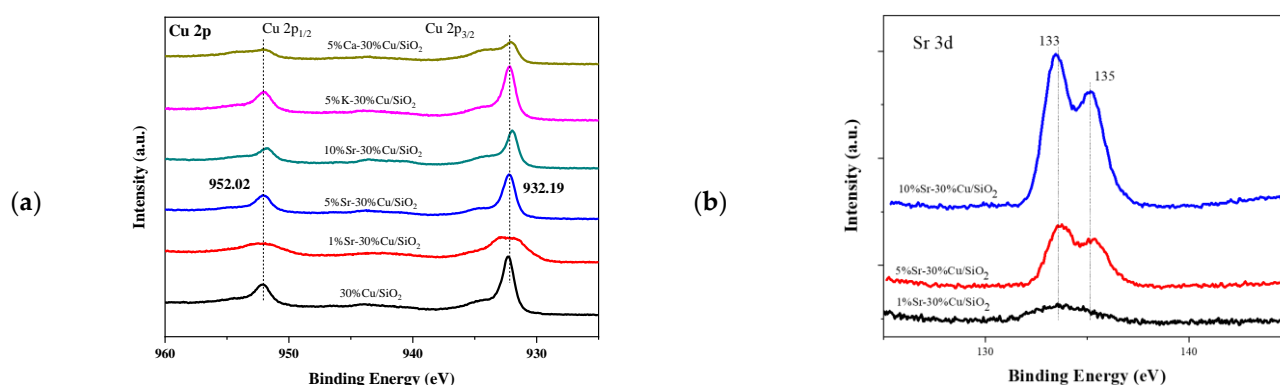


Figure 7. (a) Cu 2p spectra (b) Sr 3d XPS spectra of reduced 30%Cu/SiO₂ and xM-30%Cu/SiO₂ of as reduced catalysts.

The deconvolution performed over the recorded Cu LMM spectrum and shown in Figure 8 represents two overlapping peaks at 913.6 and 917.5 eV assigned to Cu⁺ and Cu⁰, respectively. Table 3 shows that the ratio of Cu⁺/(Cu⁰ + Cu⁺) is affected by the addition of promoters, and its value declined to 0.43 and 0.42 for 5%K-30%Cu/SiO₂ and 5%Ca-30%Cu/SiO₂, respectively, suggesting the introduction of promoters that influence the amount of Cu⁺ species on Cu/SiO₂ catalyst. Table 3 also shows that both Cu⁺ and Cu⁰ content were affected by the promoter, and, in the case of Sr-promoted catalysts, also by the amount of promoter. As a consequence, 5%Sr promoted catalysts would generate more active sites and therefore enhance the Cu dispersion as compared to other promoted and non-promoted catalysts. Moreover, further increasing Sr content would not be advantageous. This implies that there is strong interaction or bonding formed between Cu and Sr species, as previously reported in the case of other Cu-promoted catalysts, which is also a reason for enhanced dispersion and higher Cu⁺ contents [38].

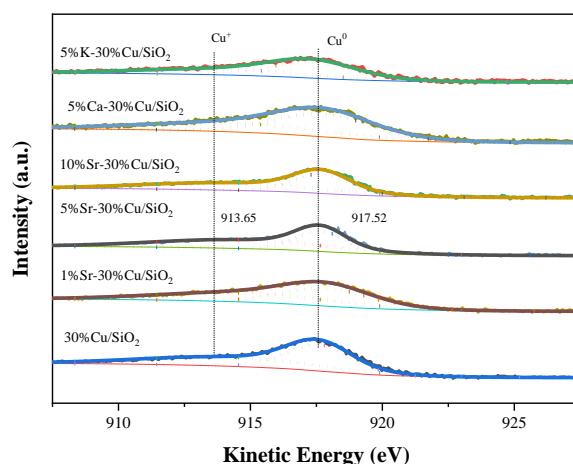


Figure 8. Cu LMM Auger spectra of reduced Cu/SiO₂ and xM-30%Cu/SiO₂ catalysts.

Table 3. Deconvolution results of XPS and Cu LMM XAES of xM-30%Cu/SiO₂ catalysts.

Catalyst	KE (eV)		AP (eV)		Cu 2p _{3/2} BE (eV)	X _{Cu⁺}
	Cu ⁺	Cu ⁰	Cu ⁺	Cu ⁰		
30%Cu/SiO ₂	913.7	917.5	1847.4	1851.3	932.3	0.48
5%K-30%Cu/SiO ₂	913.7	917.5	1847.1	1851.0	932.1	0.43
5%Ca-30%Cu/SiO ₂	913.6	917.5	1847.3	1851.3	932.0	0.42
1%Sr-30%Cu/SiO ₂	913.6	917.6	1847.5	1851.4	932.2	0.50
5%Sr-30%Cu/SiO ₂	913.7	917.5	1847.5	1851.3	932.2	0.60
10%Sr-30%Cu/SiO ₂	913.6	917.6	1847.5	1851.4	932.2	0.54

Raman spectra of all the promoted and non-promoted calcined catalysts alongside bulk CuO were also recorded and shown in Figure 9. Bulk CuO represented three characteristic bands, with a peak at 275 cm^{-1} being the most prominent. Although this band was observed in Cu/SiO₂ with no significant shift, in 5%Sr-Cu/SiO₂ catalysts a minor shift towards lower wavenumbers was observed, which could be a reflection of better metal support interaction derived from the formation of copper phyllosilicates. Similarly, in Figure 9b, the Raman spectra of spent catalysts were presented, and these catalysts were tested for long-term testing of almost 300 h. It could be seen that the characteristic peaks of both catalysts are still there, but the intensity of peaks was reduced. This implies that the crystallinity of the catalysts has been compromised as well as activity of the catalysts, hence, agglomeration of copper species is believed to be a major cause of the deactivation of Cu-based catalysts [58]. Wen et al. also reported that leaching of SiO₂ from Cu/SiO₂ catalysts could enhance rate of agglomeration of copper species after longer activity tests, therefore reducing the activity after an extensive time, and this could also be confirmed from TEM results presented in Figure 4 [59,60].

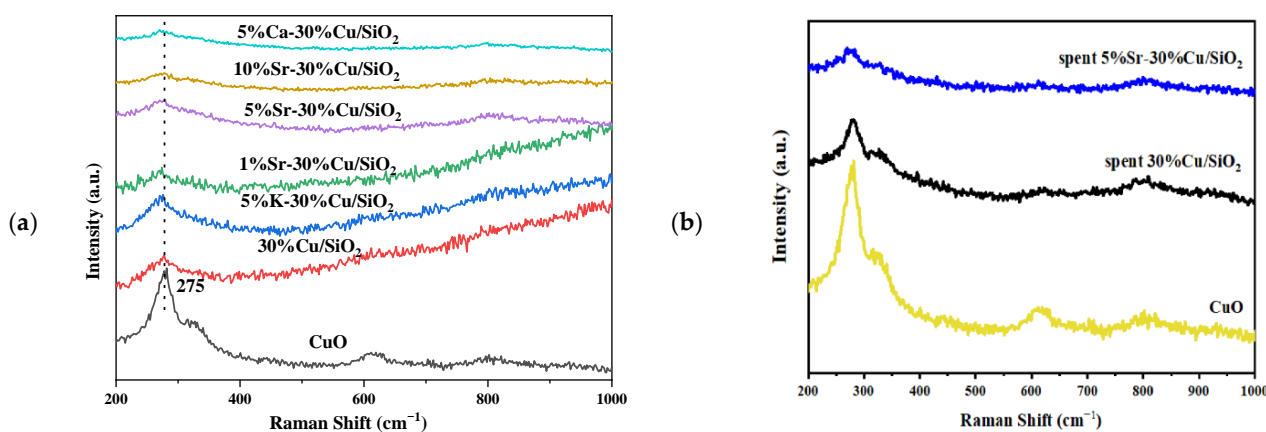


Figure 9. Raman spectra of CuO, and (a) all the promoted and non-promoted catalysts (b) spent Cu/SiO₂ and 5%Sr-30%Cu/SiO₂ catalysts.

3. Experimental

3.1. Materials

The chemicals that are used for the preparation of the catalyst were purchased reagent grade, and no further purification was done. Copper nitrate (Cu(NO₃)₂·3H₂O) [99.99%] was purchased from Aladdin (Shanghai, China), strontium nitrate (Sr(NO₃)₂) [99.5%] and calcium nitrate (Ca(NO₃)₂·4H₂O) [99.0%] were purchased from Tianjin Fuchen Chemicals Reagent Factory (Beichen, Tianjin, China), colloidal silica (LUDOX AS-40, 40 wt.% suspension in H₂O) was purchased from Sigma Aldrich (Burlington, MA, USA), and potassium nitrate (KNO₃) [AR, >99.0%] and sodium hydroxide (NaOH, AR) were purchased from Beijing Chemical Works (Yizhuang, Beijing, China).

3.2. Catalyst Preparation

The modified precipitation gel method [7] was used to prepare Cu/SiO₂ (using 30% Cu content) with different alkali and alkaline earth metals (K, Ca, Sr) as additives. 0.5 M solutions were made by adding Cu(NO₃)₂·3H₂O as Cu source, and Sr(NO₃)₂ as Sr source separately in deionized water, and mixing was done at room temperature for 30 min. 5 M NaOH was added to the mixture of Cu and Sr solutions and thoroughly mixed for 1 h, and further sonication was done for 30 min. Following that, 40% colloidal silica was added as 40 wt.% suspension in H₂O, and mixing and sonication were done for 30 min. The gel state catalyst was further mixed vigorously for 4 h at a temperature of 50 °C. Vacuum filtration and washing procedure were done (at least 4 times) until the pH of the water being collected became neutral (7.0). It was further allowed to dry for 12 h at a temperature

of 120 °C. The catalyst obtained was finally calcined at 5 °C/min from 25 to 450 °C and kept at 450 °C for 3 h. The actual 5% Sr modified and 30 wt.% Cu catalyst (5%Sr-30%Cu/SiO₂) was analyzed by inductively coupled plasma–optical emission spectroscopy (ICP-OES).

For comparing the efficiency of the prepared catalyst, more catalysts were also prepared, including 30%Cu/SiO₂, 1%Sr-30%Cu/SiO₂, 10%Sr-30%Cu/SiO₂, 5%K-30%Cu/SiO₂, 5%Ca-30%Cu/SiO₂, and 5%Sr/SiO₂. The same modified precipitation gel method as discussed above was used for the preparation of all comparing catalysts.

3.3. Catalyst Characterization

ICP-OES technique was done by using the instrument IRIS Intrepid II XSP (ThermoFisher, Waltham, MA, USA) for analyzing the concentration of copper in the catalyst. Specific surface area testing of the catalyst was determined by using a Micromeritics ASAP 2020 Plus (Micromeritics Instruments Corporation, Norcross, GA, USA) porosimetry instrument. Before taking the measurements, the samples were first treated at 350 °C for 4 h. The surface area estimation was done by the Brunauer–Emmett–Teller (BET) method while the pore size distribution was calculated by the Barrett–Joyner–Halenda (BJH) method. The phase analysis of the samples was recorded as powder X-ray diffraction (PXRD) patterns on the Rigaku Smart Lab instrument (Rigaku, Tokyo, Japan), X-ray powder diffractometer, using Cu K α (λ = 0.15406 nm) as the radiation source together with a scanning step of 10° per minute. The Scherrer equation was used for the average crystallite size calculations of reduced Cu (111) using the full width at half-maximum (FWHM) and diffraction peak at 2 θ ~43.2°. The infrared (IR) spectra of promoted and non-promoted catalysts were carried out on a Nicolet 6700 spectrometer (ThermoFisher Scientific, Waltham, MA, USA) with a spectra resolution of 4 cm^{−1} and recorded from 400 to 4000 cm^{−1}. The KBr was mixed with the sample to form self-supporting wafer. Temperature-programmed reduction (TPR) was the technique used to determine the reduction temperatures and numbers of reducible species present in the catalyst. The reduction profiles were collected on an AutochemII2920 Chemisorption (Micromeritics Instruments Corporation, Norcross, GA, USA) Apparatus (Micromeritics). In a typical procedure, 50 mg of sample was first pretreated in a quartz U-tube reactor at 120 °C for 1 h under He atmosphere, then cooled down to room temperature. After it reaches room temperature under helium, 10% H₂-Ar was introduced into the tubular reactor, and temperature was ramped from 10 °C/min to 500 °C. H₂ temperature-programmed desorption (H₂-TPD) and H₂ temperature-programmed reduction (H₂-TPR) profiles were collected on the same equipment. Initially, the sample was reduced at 350 °C in 10% H₂-Ar atmosphere for 4 h and then the adsorption was conducted at 50 °C for 1 h, followed by high purity purge by argon. Finally, desorption of H₂ was measured at a linear heating program from 50 °C to 800 °C at 10 °C/min. The number of the metallic copper surface of catalyst was determined by N₂O-titration at 90 °C, followed by CO-TPD in the above-described apparatus according to the procedure mentioned elsewhere by Van Der Grift et al. [61], assuming that Cu⁺ ions and Cu⁰ atoms occupy identical areas (1.47 × 10¹⁹ copper atoms/m²), as reported previously [28]. The surface copper and promoting metal species of the catalysts were detected by X-ray photoelectron spectroscopy (XPS), however, the ratio of different copper species was obtained by Auger electron spectroscopy (XAES), where Al K α X-ray ($h\nu$ = 1486.6 eV) radiation source was used on an ESCA Lab220i-XL (ThermoFisher Scientific, Waltham, MA, USA) electron spectrometer (VG Scientific). First, the catalysts were activated by reducing at 350 °C for 4 h in pure hydrogen and were later compressed into a thin disk in a glovebox under appropriate pressure and transferred to a sealed container for XPS analysis. C1s peak (284.6 eV) was used to calibrate the binding energies (BE). FE-SEM images were taken using JEOL JSM-7600 (Pleasanton, CA, USA) at 15 kV, and the energy dispersion spectra were studied using an EFI Verios G4 scanning electron microscope equipped with Thermo NS7 (Waltham, MA, USA) energy dispersion spectrometer (EDS). A transmission electron microscope (JEM-2100, Pleasanton, CA, USA) was operated at 200 kV to characterize the morphology and structure of the samples, whereas EDS mapping in STEM mode reveals the elemental dispersion. Similarly,

a scanning electron microscope (Hitachi S-4800, Chiyoda, Tokyo, Japan) equipped with energy dispersive X-ray (EDX) was also used to determine surface properties and chemical composition of the catalysts.

3.4. Catalyst Tests

The catalytic performance of Vapor phase MA hydrogenation was evaluated using a stainless-steel fixed-bed tubular microreactor installed vertically in a furnace, as shown in Figure 10. In a typical run, about 1.0 g 40–60 mesh size catalyst was loaded in the center of the reactor with both sides plugged with glass wool, and the rest of the reactor was packed with quartz powder (40–60 mesh). Before the hydrogenation reaction, the catalyst was activated in situ by heating at steady-state ($2\text{ }^{\circ}\text{C}/\text{min}$) from room temperature to $350\text{ }^{\circ}\text{C}$ under pure hydrogen flow for 4 h. In the next step, the reactor was cooled down to achieve the required reaction temperature ($180\text{ }^{\circ}\text{C}$ to $280\text{ }^{\circ}\text{C}$) and the system was pressurized slowly to targeted pressure (2.0–3.0 MPa) to test all the promoted and non-promoted xM-30%Cu/SiO₂ catalysts. MA was fed into the pre-heater with a high-pressure precision pump, where it was evaporated and pre-mixed with H₂ and carried into the reactor with H₂ flow. Standard reaction conditions were H₂/MA ratio of 15, GHSV fixed at 3000 h^{-1} , LHSV in the range of $0.5\text{--}4.0\text{ h}^{-1}$, temperature $250\text{ }^{\circ}\text{C}$, and pressure at 2.5 MPa. The product stream (a mixture of methanol, ethanol, unreacted MA, and H₂) was passed through a condenser, and separated product gases were analyzed by an online gas chromatograph, whereas separated liquid products were analyzed by a gas chromatograph device (Ruihong SP-7890, Tengzhou, Shandong, China) equipped with a flame ionization detector (FID) and an OV1701 capillary column. Shimadzu GC-MS (QP2010, Nakagyo-ku, Kyoto, Japan) was used to identify the contents of product mixture. The internal standard method with iso-butanol as the internal standard was used to calculate the conversion of MA and selectivity of ethanol. Once the system achieved steady-state, three readings were taken and the error bar was calculated.

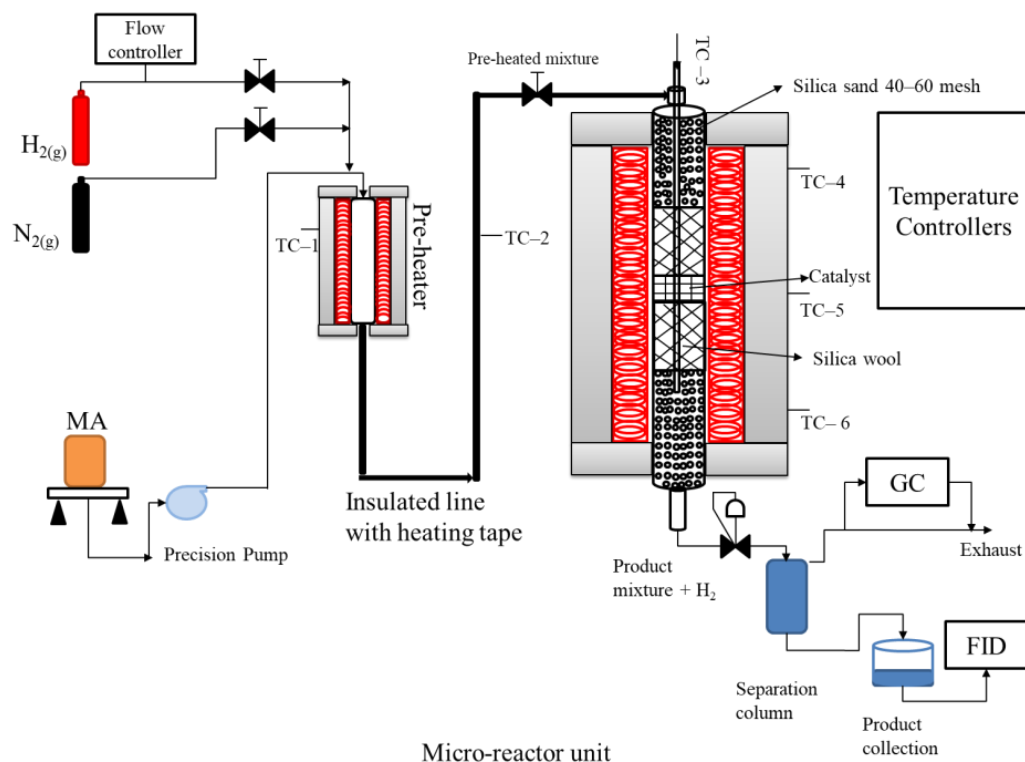


Figure 10. Schematic of fixed-bed microreactor system.

The conversion of MA (%), selectivity (%), and yield (%) of ethanol were calculated using the following equations [29]:

$$\text{Conversion of MA (\%)} = \frac{\text{moles of MA (in)} - \text{moles of MA (out)}}{\text{moles of MA (in)}} \times 100 \quad (1)$$

$$\text{Selectivity of ethanol (\%)} = \frac{\text{moles of ethanol (out)}}{\text{moles of MA (in)} - \text{moles of MA (out)}} \times 100 \quad (2)$$

$$\text{Yield of ethanol (\%)} = \frac{\text{moles of ethanol (out)}}{\text{moles of MA (in)}} \times 100 \quad (3)$$

3.5. Catalytic Performance and Stability

Table 4 summarizes the results of catalytic hydrogenation of MA over different catalysts. According to results tabulated in Table 4, 5%Sr/SiO₂ was showing almost no activity for hydrogenation of MA to ethanol, suggesting that Sr has no active site for the reaction. The promotion with alkali and alkaline earth metals (K, Ca, Sr) enhanced the catalytic activity of Cu/SiO₂ catalyst, with Sr promoting catalysts outperforming the rest of the promoted and non-promoting catalysts in terms of MA conversion (95.8%) and selectivity for ethanol (96.2%). Similarly, the addition of 5% K and 5% Ca also increased MA conversion to 92.2% and 91.1% and selectivity to 91.3% and 90.2%, respectively. It can be elucidated from experimental results that catalyst promotion with 1% strontium initially increased MA conversion and ethanol selectivity, but further increasing it to 10% significantly reduced the catalytic performance at similar reaction conditions. Similarly, spacetime yield (STY) value reaches a maximum with 5% Sr-promoted catalyst, e.g., 1.07 g_{Ethanol}/(g_{cat} h), whereas in 10% Sr-promoted catalyst this value declines to 0.89 g_{Ethanol}/(g_{cat} h), showing that a further increase in Sr content from optimum will reduce the performance of the catalyst.

Table 4. Catalytic performance for hydrogenation of MA over xM-30%Cu/SiO₂ catalysts.

Catalyst	MA Conversion/ % ^a	Ethanol Selectivity/ % ^a	Yield/ % ^a	STY/ g _{Ethanol} /(g _{cat} h) ^a
30%Cu/SiO ₂	90.8	86.3	78.4	0.91
5%K-30%Cu/SiO ₂	92.2	91.3	84.2	0.97
5%Ca-30%Cu/SiO ₂	91.1	90.2	82.2	0.95
1%Sr-30%Cu/SiO ₂	91.8	91.2	83.7	0.97
5%Sr-30%Cu/SiO ₂	95.8	96.2	92.2	1.07
10%Sr-30%Cu/SiO ₂	87.7	88.0	77.3	0.89
5%Sr/SiO ₂	0	0	0	0

^a Reaction condition: T = 250 °C, P = 2.5 MPa, GHSV = 3000 h^{−1}, LHSV = 1 h^{−1}.

3.5.1. Effect of Reaction Temperature

Figure 11 presented the MA conversion, and ethanol selectivity for 5%Sr-30%Cu/SiO₂ and 30%Cu/SiO₂ at different reaction temperatures, liquid hourly space velocity (LHSV), and pressures. As shown in Figure 11a, the two catalysts were further evaluated to check the effect of temperature on the activity of the catalyst, and therefore the temperature was changed from 190 °C to 280 °C. Both conversion and selectivity improved significantly throughout temperature range in Sr-promoted catalyst. It was observed that MA conversion and selectivity of ethanol increased by almost 50% when the temperature was increased from 190 °C to 220 °C in the case of Sr-promoted catalyst. It was also evident from data collected that activity was highest in terms of percentage yield (92.2%) at 250 °C, although MA conversion further increased a few points at 280 °C at the stake of ethanol selectivity, which was due to possible side reactions that occurred at higher temperatures and the consequent formation of byproducts, as was reported in our previous work [29].

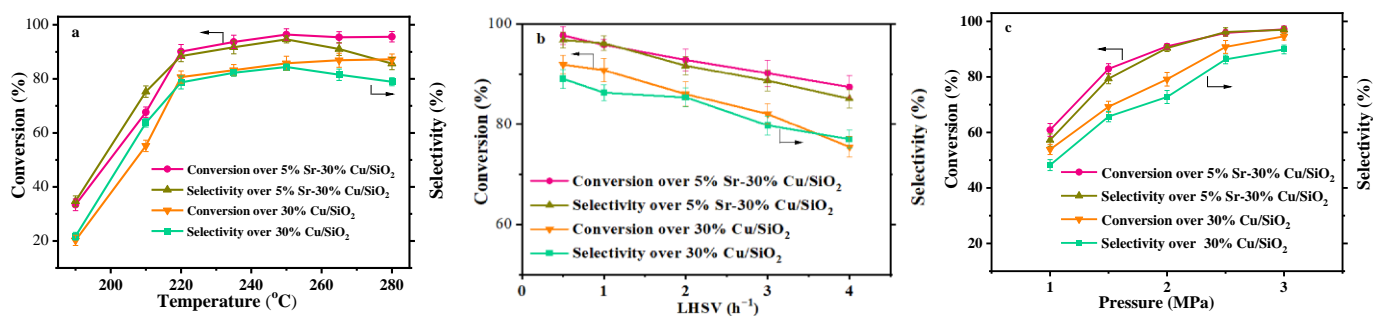


Figure 11. Effect of reaction conditions on reaction activity. (a) Effect of reaction temperature, $P(\text{H}_2) = 2.5 \text{ MPa}$, $\text{LHSV} = 1 \text{ h}^{-1}$, $\text{GHSV} = 3000 \text{ h}^{-1}$. (b) Effect of liquid hourly space velocity (LHSV), $T = 250 \text{ }^\circ\text{C}$, $P(\text{H}_2) = 2.5 \text{ MPa}$, $\text{GHSV} = 3000 \text{ h}^{-1}$. (c) Effect of pressure, $T = 250 \text{ }^\circ\text{C}$, $\text{H}_2/\text{MA} = 15$, $\text{LHSV} = 1 \text{ h}^{-1}$.

3.5.2. Effect of Liquid Hourly Space Velocity

Figure 11b shows the effect of LHSV on MA conversion and ethanol selectivity, which is another important factor studied. As shown, LHSV varied from 0.5 h^{-1} to 4.0 h^{-1} , and the highest MA conversion and ethanol selectivity were achieved at 0.5 h^{-1} (97.7% and 96.8%, respectively). A slight decline at 1.0 h^{-1} in 5%Sr-30%Cu/SiO₂ catalyst was observed, which was still 6% higher than the non-promoted catalyst. At higher LHSV conditions, MA conversion, and the selectivity of ethanol, the 5%Sr-30%Cu/SiO₂ catalyst was 87.4% and 85.1%, respectively, whereas, in non-promoted catalysts, these figures stand at 75.5% and 77.0%. This decrease was also evident in our previous studies [22,29,30]. It suggested that activity of the promoted catalyst was incredibly stable, even at the highest LHSV (4.0 h^{-1}) as compared to the non-promoted catalyst, and it could be due to more active sites available for reaction, even under extreme conditions.

3.5.3. Effect of Pressure

The effect of pressure on MA conversion and ethanol selectivity was observed at a reaction temperature of $250 \text{ }^\circ\text{C}$, with pressure from 1.0–3.0 MPa and 1.0 h^{-1} LHSV, as shown in Figure 11c. MA conversion enhanced with an increase in pressure and selectivity of ethanol also demonstrated a similar trend, with maximum MA conversion of 97.1% and selectivity of ethanol 96.9% at 3.0 MPa in Sr-promoted catalyst. This study has reflected that an increase in pressure from 2.5 MPa to 3.0 MPa had a minor effect on MA conversion and selectivity of ethanol.

3.5.4. Catalytic Stability

The comparison of long-term stability of best-performing promoted catalyst with non-promoted catalyst is of tremendous significance from both academic and industrial perspectives. The comparison of long-term catalytic stability of 5%Sr-30%Cu/SiO₂ and non-promoted 30%Cu/SiO₂ is presented in Figure 12. The Sr-promoted catalyst exhibited excellent stability and performed exceptionally for more than 300 h continuously in terms of MA conversion and selectivity for ethanol, which remained at 95% and 96%, respectively. However, a time-dependent decrease in the activity of the non-promoted catalyst was observed with a slow decline after 150 h, and this could be due to agglomeration of Cu species, as was evident from an increase in mean particle size to 7.07 nm of spent Cu/SiO₂ catalyst, as shown in Figure 4e. Many previous works had reported that the inactivation of the Cu-based catalyst was mainly caused by the agglomeration of copper species; thus, we focused on the observations of agglomerative phases by TEM and Raman to verify this phenomenon [59,60]. It also could be found that after long-term testing of catalysts, a major loss to catalyst activity in the case of 30%Cu/SiO₂ catalyst was due to agglomeration of Cu species, which could also be confirmed from TEM of spent catalysts presented in TEM analysis. However, there is a very minute effect observed in the case of 5%Sr-30%Cu/SiO₂

catalyst, hence the almost negligible effect in activity. Furthermore, this decline in activity became clearer from 250 h for both MA conversion and selectivity of ethanol.

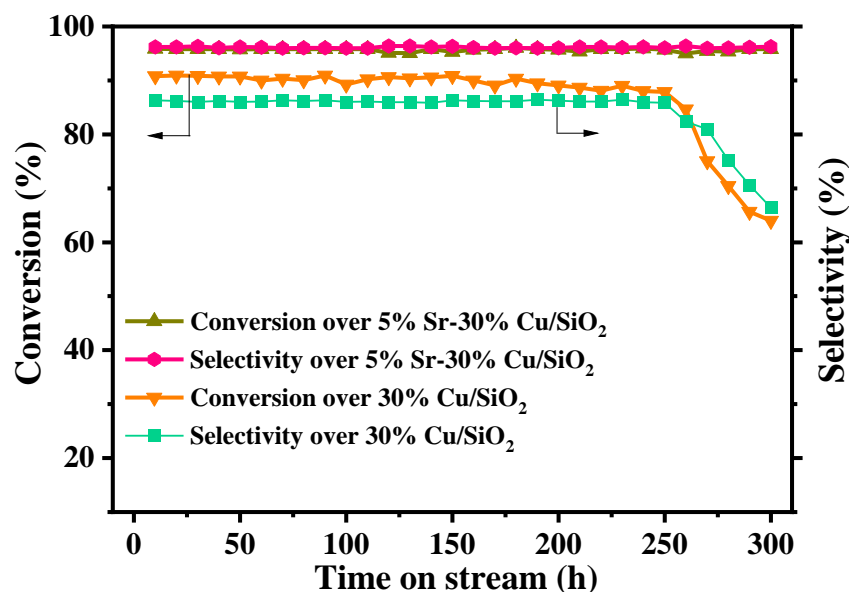


Figure 12. Long-term catalytic performance of 30%Cu/SiO₂ and 5%Sr-30% Cu/SiO₂ catalysts as a function of reaction time at, T = 250 °C, P(H₂) = 2.5 MPa, LHSV = 1 h^{−1}, GHSV = 3000 h^{−1}.

4. Conclusions

This study reported a series of selective alkali and alkaline earth metals (K, Ca, Sr) promoted Cu/SiO₂ catalyst prepared by a modified precipitation-gel method. Furthermore, promotion with an appropriate amount of strontium (5%Sr-30%Cu/SiO₂) further improved the catalytic activity, i.e., conversion and selectivity from 90.8% and 86.3% to 95.8% and 96.2%, respectively, and stability to more than 300 h for the hydrogenation of MA to ethanol. The interaction between copper ions, promoters, and support surface was significantly enhanced, which resulted in higher copper surface area, improvement in reducibility, and other physiochemical properties. Compared to all the reported xM-30%Cu/SiO₂ catalysts, 5%Sr-30%Cu/SiO₂ exhibited superior catalytic activity under similar reaction conditions for hydrogenation of MA to ethanol. The maximum molar ratio of Cu⁺/(Cu⁺ + Cu⁰) obtained by changing strontium content to 5% Sr could have led to the highest catalytic performance. In addition, several characterizations showed that promotion with 5%Sr not only restrained the agglomeration but also controlled the valence change of cupreous species during a long-term test, hence displaying promising characteristics for industrialization.

Author Contributions: Conceptualization, M.N.Y., C.L. and Z.R.; methodology, M.N.Y., Z.R.; software, M.N.Y., Z.R.; validation, E.W. and C.L.; formal analysis, M.N.Y.; investigation, M.N.Y., C.L. and Z.R.; resources, C.L., M.N.Y.; data curation, M.N.Y. and Z.R.; writing—original draft preparation, M.N.Y.; writing—review and editing, M.N.Y., Z.R., C.L., E.W.; supervision, C.L.; project administration, C.L. and J.L.; funding acquisition, C.L., E.W. and J.L. All authors have read and agreed to the published version of the manuscript.

Funding: This research received no external funding.

Data Availability Statement: Not applicable.

Acknowledgments: The authors are grateful to CAS-TWAS President's Fellowship program for providing a research opportunity.

Conflicts of Interest: The authors declare no conflict of interest

References

1. Roehr, M. *The Biotechnology of Ethanol: Classical and Future Applications*; Wiley-VCH Verlag GmbH: Weinheim, Germany, 2000, ISBN 9783527602346.
2. Jiao, J.; Li, J.; Bai, Y. Ethanol as a Vehicle Fuel in China: A Review from the Perspectives of Raw Material Resource, Vehicle, and Infrastructure. *J. Clean. Prod.* **2018**, *180*, 832–845. [\[CrossRef\]](#)
3. Dueso, C.; Ortiz, M.; Abad, A.; García-Labiano, F.; de Diego, L.F.; Gayán, P.; Adánez, J. Reduction and Oxidation Kinetics of Nickel-Based Oxygen-Carriers for Chemical-Looping Combustion and Chemical-Looping Reforming. *Chem. Eng. J.* **2012**, *188*, 142–154. [\[CrossRef\]](#)
4. Li, X.; San, X.; Zhang, Y.; Ichii, T.; Meng, M.; Tan, Y.; Tsubaki, N. Direct Synthesis of Ethanol from Dimethyl Ether and Syngas over Combined H-Mordenite and Cu/ZnO Catalysts. *ChemSusChem* **2010**, *3*, 1192–1199. [\[CrossRef\]](#)
5. Wang, S.; Guo, W.; Wang, H.; Zhu, L.; Yin, S.; Qiu, K. Effect of the Cu/SBA-15 Catalyst Preparation Method on Methyl Acetate Hydrogenation for Ethanol Production. *N. J. Chem.* **2014**, *38*, 2792. [\[CrossRef\]](#)
6. Ye, C.; Guo, C.; Sun, C.; Zhang, Y. Effect of Mn Doping on the Activity and Stability of Cu-SiO₂ Catalysts for the Hydrogenation of Methyl Acetate to Ethanol. *RSC Adv.* **2016**, *6*, 113796–113802. [\[CrossRef\]](#)
7. Huang, Z.; Cui, F.; Kang, H.; Chen, J. Highly Dispersed Silica-Supported Copper Nanoparticles Prepared by Precipitation–Gel Method: A Simple but Efficient and Stable Catalyst for Glycerol Hydrogenolysis. *Chem. Mater.* **2008**, *20*, 5090–5099. [\[CrossRef\]](#)
8. Ye, C.-L.; Guo, C.-L.; Zhang, J.-L. Highly Active and Stable CeO₂–SiO₂ Supported Cu Catalysts for the Hydrogenation of Methyl Acetate to Ethanol. *Fuel Process. Technol.* **2016**, *143*, 219–224. [\[CrossRef\]](#)
9. Huang, X.; Ma, M.; Miao, S.; Zheng, Y.; Chen, M.; Shen, W. Hydrogenation of Methyl Acetate to Ethanol over a Highly Stable Cu/SiO₂ Catalyst: Reaction Mechanism and Structural Evolution. *Appl. Catal. A Gen.* **2017**, *531*, 79–88. [\[CrossRef\]](#)
10. Chen, L.-F.; Guo, P.-J.; Qiao, M.-H.; Yan, S.-R.; Li, H.-X.; Shen, W.; Xu, H.-L.; Fan, K.-N. Cu/SiO₂ Catalysts Prepared by the Ammonia-Evaporation Method: Texture, Structure, and Catalytic Performance in Hydrogenation of Dimethyl Oxalate to Ethylene Glycol. *J. Catal.* **2008**, *257*, 172–180. [\[CrossRef\]](#)
11. Yin, A.; Guo, X.; Fan, K.; Dai, W.-L. Ion-Exchange Temperature Effect on Cu/HMS Catalysts for the Hydrogenation of Dimethyl Oxalate to Ethylene Glycol. *ChemCatChem* **2010**, *2*, 206–213. [\[CrossRef\]](#)
12. Yin, A.; Guo, X.; Dai, W.L.; Li, H.; Fan, K. Highly Active and Selective Copper-Containing HMS Catalyst in the Hydrogenation of Dimethyl Oxalate to Ethylene Glycol. *Appl. Catal. A Gen.* **2008**, *349*, 91–99. [\[CrossRef\]](#)
13. Di, W.; Cheng, J.; Tian, S.; Li, J.; Chen, J.; Sun, Q. Synthesis and Characterization of Supported Copper Phyllosilicate Catalysts for Acetic Ester Hydrogenation to Ethanol. *Appl. Catal. A Gen.* **2016**, *510*, 244–259. [\[CrossRef\]](#)
14. He, Z.; Lin, H.; He, P.; Yuan, Y. Effect of Boric Oxide Doping on the Stability and Activity of a Cu-SiO₂ catalyst for Vapor-Phase Hydrogenation of Dimethyl Oxalate to Ethylene Glycol. *J. Catal.* **2011**, *277*, 54–63. [\[CrossRef\]](#)
15. Zhong, K.; Wang, X. The Influence of Different Precipitants on the Copper-Based Catalysts for Hydrogenation of Ethyl Acetate to Ethanol. *Int. J. Hydrogen Energy* **2014**, *39*, 10951–10958. [\[CrossRef\]](#)
16. Yang, D.; Sararuk, C.; Suzuki, K.; Li, Z.; Li, C. Effect of Calcination Temperature on the Catalytic Activity of VPO for Aldol Condensation of Acetic Acid and Formalin. *Chem. Eng. J.* **2016**, *300*, 160–168. [\[CrossRef\]](#)
17. Lin, D.; Zhang, Q.; Qin, Z.; Li, Q.; Feng, X.; Song, Z.; Cai, Z.; Liu, Y.; Chen, X.; Chen, D.; et al. Reversing Titanium Oligomer Formation towards High-Efficiency and Green Synthesis of Titanium-Containing Molecular Sieves. *Angew. Chem. Int. Ed.* **2021**, *60*, 3443–3448. [\[CrossRef\]](#)
18. Runeberg, J.; Baiker, A.; Kijenski, J. Copper Catalyzed Amination of Ethylene Glycol. *Appl. Catal.* **1985**, *17*, 309–319. [\[CrossRef\]](#)
19. Montassier, C.; Giraud, D.; Barbier, J. Polyol Conversion by Liquid Phase Heterogeneous Catalysis over Metals. *Prep. Catal. V-Sci. Bases Prep. Heterog. Catal. Proc. Fifth Int. Symp.* **1988**, *41*, 165–170.
20. Brands, D.S.; Poels, E.K.; Blik, A. Ester Hydrogenolysis over Promoted Cu/SiO₂ Catalysts. *Appl. Catal. A Gen.* **1999**, *184*, 279–289. [\[CrossRef\]](#)
21. Wang, Y.; Liao, J.; Zhang, J.; Wang, S.; Zhao, Y.; Ma, X. Hydrogenation of Methyl Acetate to Ethanol by Cu/ZnO Catalyst Encapsulated in SBA-15. *AIChE J.* **2017**, *63*, 2839–2849. [\[CrossRef\]](#)
22. Ren, Z.; Younis, M.N.; Zhao, H.; Li, C.; Yang, X.; Wang, E.; Wang, G. Silver Modified Cu/SiO₂ Catalyst for the Hydrogenation of Methyl Acetate to Ethanol. *Chin. J. Chem. Eng.* **2020**, *28*, 1612–1622. [\[CrossRef\]](#)
23. Yan, H.; Li, S.; Feng, X.; Lu, J.; Zheng, X.; Li, R.; Zhou, X.; Chen, X.; Liu, Y.; Chen, D.; et al. Rational Screening of Metal Catalysts for Selective Oxidation of Glycerol to Glyceric Acid from Microkinetic Analysis. *AIChE J.* **2023**, *69*, e17868. [\[CrossRef\]](#)
24. Yan, H.; Zhao, M.; Feng, X.; Zhao, S.; Zhou, X.; Li, S.; Zha, M.; Meng, F.; Chen, X.; Liu, Y.; et al. PO₄^{3−} Coordinated Robust Single-Atom Platinum Catalyst for Selective Polyol Oxidation. *Angew. Chem. Int. Ed.* **2022**, *61*, e202116059. [\[CrossRef\]](#)
25. Wang, Y.; Shen, Y.; Zhao, Y.; Lv, J.; Wang, S.; Ma, X. Insight into the Balancing Effect of Active Cu Species for Hydrogenation of Carbon–Oxygen Bonds. *ACS Catal.* **2015**, *5*, 6200–6208. [\[CrossRef\]](#)
26. Huang, Z.; Liu, H.; Cui, F.; Zuo, J.; Chen, J.; Xia, C. Effects of the Precipitation Agents and Rare Earth Additives on the Structure and Catalytic Performance in Glycerol Hydrogenolysis of Cu/SiO₂ catalysts Prepared by Precipitation-Gel Method. *Catal. Today* **2014**, *234*, 223–232. [\[CrossRef\]](#)
27. Qin, H.; Guo, C.; Sun, C.; Zhang, J. Influence of the Support Composition on the Hydrogenation of Methyl Acetate over Cu/MgO-SiO₂ Catalysts. *J. Mol. Catal. A: Chem.* **2015**, *409*, 79–84. [\[CrossRef\]](#)

28. Zhao, Y.; Shan, B.; Wang, Y.; Zhou, J.; Wang, S.; Ma, X. An Effective CuZn-SiO₂ Bimetallic Catalyst Prepared by Hydrolysis Precipitation Method for the Hydrogenation of Methyl Acetate to Ethanol. *Ind. Eng. Chem. Res.* **2018**, *57*, 4526–4534. [\[CrossRef\]](#)
29. Ren, Z.; Younis, M.N.; Li, C.; Li, Z.; Yang, X.; Wang, G. Highly Active Ce, Y, La-Modified Cu/SiO₂ Catalysts for Hydrogenation of Methyl Acetate to Ethanol. *RSC Adv.* **2020**, *10*, 5590–5603. [\[CrossRef\]](#)
30. Ren, Z.; Younis, M.N.; Wu, H.; Li, C.; Yang, X.; Wang, G. Design and Synthesis of La-Modified Copper Phyllosilicate Nanotubes for Hydrogenation of Methyl Acetate to Ethanol. *Catal. Lett.* **2021**, *151*, 3089–3102. [\[CrossRef\]](#)
31. Zhou, J.; Guo, L.; Guo, X.; Mao, J.; Zhang, S. Selective Hydrogenolysis of Glycerol to Propanediols on Supported Cu-Containing Bimetallic Catalysts. *Green Chem.* **2010**, *12*, 1835–1843. [\[CrossRef\]](#)
32. Yaseen, M.; Shakirullah, M.; Ahmad, I.; Rahman, A.U.; Rahman, F.U.; Usman, M.; Razzaq, R. Simultaneous Operation of Dibenzothiophene Hydrodesulfurization and Methanol Reforming Reactions over Pd Promoted Alumina Based Catalysts. *J. Fuel Chem. Technol.* **2012**, *40*, 714–720. [\[CrossRef\]](#)
33. Muhammad, Y.; Rashid, H.U.; Subhan, S.; Rahman, A.U.; Sahibzada, M.; Tong, Z. Boosting the Hydrodesulfurization of Dibenzothiophene Efficiency of Mn Decorated (Co/Ni)-Mo/Al₂O₃ Catalysts at Mild Temperature and Pressure by Coupling with Phosphonium Based Ionic Liquids. *Chem. Eng. J.* **2019**, *375*, 121957. [\[CrossRef\]](#)
34. Muhammad, Y.; Rahman, A.U.; Rashid, H.U.; Sahibzada, M.; Subhan, S.; Tong, Z. Hydrodesulfurization of Dibenzothiophene Using Pd-Promoted Co-Mo/Al₂O₃ and Ni-Mo/Al₂O₃ Catalysts Coupled with Ionic Liquids at Ambient Operating Conditions. *RSC Adv.* **2019**, *9*, 10371–10385. [\[CrossRef\]](#) [\[PubMed\]](#)
35. Liu, H.; Huang, Z.; Kang, H.; Li, X.; Xia, C.; Chen, J.; Liu, H. Efficient Bimetallic NiCu-SiO₂ Catalysts for Selective Hydrogenolysis of Xylitol to Ethylene Glycol and Propylene Glycol. *Appl. Catal. B: Environ.* **2018**, *220*, 251–263. [\[CrossRef\]](#)
36. Yan, H.; Qin, H.; Feng, X.; Jin, X.; Liang, W.; Sheng, N.; Zhu, C.; Wang, H.; Yin, B.; Liu, Y.; et al. Synergistic Pt/MgO/SBA-15 Nanocatalysts for Glycerol Oxidation in Base-Free Medium: Catalyst Design and Mechanistic Study. *J. Catal.* **2019**, *370*, 434–446. [\[CrossRef\]](#)
37. Zhu, Y.-M.; Shi, L. Zn Promoted Cu–Al Catalyst for Hydrogenation of Ethyl Acetate to Alcohol. *J. Ind. Eng. Chem.* **2014**, *20*, 2341–2347. [\[CrossRef\]](#)
38. Zheng, X.; Lin, H.; Zheng, J.; Duan, X.; Yuan, Y. Lanthanum Oxide-Modified Cu/SiO₂ as a High-Performance Catalyst for Chemoselective Hydrogenation of Dimethyl Oxalate to Ethylene Glycol. *ACS Catal.* **2013**, *3*, 2738–2749. [\[CrossRef\]](#)
39. Ying, J.; Han, X.; Ma, L.; Lu, C.; Feng, F.; Zhang, Q.; Li, X. Effects of Basic Promoters on the Catalytic Performance of Cu/SiO₂ in the Hydrogenation of Dimethyl Maleate. *Catalysts* **2019**, *9*, 704. [\[CrossRef\]](#)
40. Gluhoi, A.C.; Nieuwenhuys, B.E. Structural and Chemical Promoter Effects of Alkali (Earth) and Cerium Oxides in CO Oxidation on Supported Gold. *Catal. Today* **2007**, *122*, 226–232. [\[CrossRef\]](#)
41. Gluhoi, A.C.; Bogdanchikova, N.; Nieuwenhuys, B.E. Alkali (Earth)-Doped Au/Al₂O₃ Catalysts for the Total Oxidation of Propene. *J. Catal.* **2005**, *232*, 96–101. [\[CrossRef\]](#)
42. Yang, D.; Li, J.; Wen, M.; Song, C. Enhanced Activity of Ca-Doped Cu/ZrO₂ for Nitrogen Oxides Reduction with Propylene in the Presence of Excess Oxygen. *Catal. Today* **2008**, *139*, 2–7. [\[CrossRef\]](#)
43. Pellegrini, R.; Leofanti, G.; Agostini, G.; Bertinetti, L.; Bertarione, S.; Groppo, E.; Zecchina, A.; Lamberti, C. Influence of K-Doping on a Pd/SiO₂-Al₂O₃ Catalyst. *J. Catal.* **2009**, *267*, 40–49. [\[CrossRef\]](#)
44. Evans, J.W.; Wainwright, M.S.; Bridgewater, A.J.; Young, D.J. On the Determination of Copper Surface Area by Reaction with Nitrous Oxide. *Appl. Catal.* **1983**, *7*, 75–83. [\[CrossRef\]](#)
45. Zhang, B.; Zhu, Y.; Ding, G.; Zheng, H.; Li, Y. Modification of the Supported Cu/SiO₂ Catalyst by Alkaline Earth Metals in the Selective Conversion of 1,4-Butanediol to γ -Butyrolactone. *Appl. Catal. A Gen.* **2012**, *443–444*, 191–201. [\[CrossRef\]](#)
46. Wang, Z.; Wang, W.; Lu, G. Studies on the Active Species and on Dispersion of Cu in Cu/SiO₂ and Cu/Zn/SiO₂ for Hydrogen Production via Methanol Partial Oxidation. *Int. J. Hydrogen Energy* **2003**, *28*, 151–158. [\[CrossRef\]](#)
47. Toupance, T.; Kermarec, M.; Lambert, J.-F.; Louis, C. Conditions of Formation of Copper Phyllosilicates in Silica-Supported Copper Catalysts Prepared by Selective Adsorption. *J. Phys. Chem. B* **2002**, *106*, 2277–2286. [\[CrossRef\]](#)
48. To, D.T.; Lin, Y.C. Copper Phyllosilicates-Derived Catalysts in the Production of Alcohols from Hydrogenation of Carboxylates, Carboxylic Acids, Carbonates, Formyls, and CO₂: A Review. *Catalysts* **2021**, *11*, 255. [\[CrossRef\]](#)
49. Maul, J.; Brito, A.S.; de Oliveira, A.L.M.; Lima, S.J.G.; Maurera, M.A.M.A.; Keyson, D.; Souza, A.G.; Santos, I.M.G. Influence of the Synthesis Media in the Properties of CuO Obtained by Microwave-Assisted Hydrothermal Method. *J. Therm. Anal. Calorim.* **2011**, *106*, 519–523. [\[CrossRef\]](#)
50. Lu, L.; Huang, X. Room Temperature Electrochemical Synthesis of CuO Flower-like Microspheres and Their Electrooxidative Activity towards Hydrogen Peroxide. *Microchim. Acta* **2011**, *175*, 151. [\[CrossRef\]](#)
51. Hou, X.; Zhao, J.; Liu, J.; Han, Y.; Pei, Y.; Ren, J. Activated Carbon Aerogel Supported Copper Catalysts for the Hydrogenation of Methyl Acetate to Ethanol: Effect of KOH Activation. *N. J. Chem.* **2019**, *43*, 9430–9438. [\[CrossRef\]](#)
52. Wilmer, H.; Genger, T.; Hinrichsen, O. The Interaction of Hydrogen with Alumina-Supported Copper Catalysts: A Temperature-Programmed Adsorption/Temperature-Programmed Desorption/Isotopic Exchange Reaction Study. *J. Catal.* **2003**, *215*, 188–198. [\[CrossRef\]](#)
53. Scholten, J.J.F.; Pijpers, A.P.; Hustings, A.M.L. Surface Characterization of Supported and Unsupported Hydrogenation Catalysts. *Catal. Rev.* **1985**, *27*, 151–206. [\[CrossRef\]](#)

54. Dong, X.; Zhang, H.-B.; Lin, G.-D.; Yuan, Y.-Z.; Tsai, K.R. Highly Active CNT-Promoted Cu-ZnO-Al₂O₃ Catalyst for Methanol Synthesis from H₂/CO/CO₂. *Catal. Lett.* **2003**, *85*, 237–246. [[CrossRef](#)]
55. Tu, Y.J.; Chen, Y.W. Effects of Alkali Metal Oxide Additives on Cu/SiO₂ Catalyst in the Dehydrogenation of Ethanol. *Ind. Eng. Chem. Res.* **2001**, *40*, 5889–5893. [[CrossRef](#)]
56. Gong, J.; Yue, H.; Zhao, Y.; Zhao, S.; Zhao, L.; Lv, J.; Wang, S.; Ma, X. Synthesis of Ethanol via Syngas on Cu/SiO₂ Catalysts with Balanced Cu⁰–Cu⁺ Sites. *J. Am. Chem. Soc.* **2012**, *134*, 13922–13925. [[CrossRef](#)]
57. Yin, A.; Guo, X.; Dai, W.-L.; Fan, K. The Nature of Active Copper Species in Cu-HMS Catalyst for Hydrogenation of Dimethyl Oxalate to Ethylene Glycol: New Insights on the Synergetic Effect between Cu⁰ and Cu⁺. *J. Phys. Chem. C* **2009**, *113*, 11003–11013. [[CrossRef](#)]
58. Shen, J.; Rao, C.; Fu, Z.; Feng, X.; Liu, J.; Fan, X.; Peng, H.; Xu, X.; Tan, C.; Wang, X. The Influence on the Structural and Redox Property of CuO by Using Different Precursors and Precipitants for Catalytic Soot Combustion. *Appl. Surf. Sci.* **2018**, *453*, 204–213. [[CrossRef](#)]
59. Wen, C.; Cui, Y.; Dai, W.L.; Xie, S.; Fan, K. Solvent Feedstock Effect: The Insights into the Deactivation Mechanism of Cu/SiO₂ Catalysts for Hydrogenation of Dimethyl Oxalate to Ethylene Glycol. *Chem. Commun.* **2013**, *49*, 5195–5197. [[CrossRef](#)] [[PubMed](#)]
60. Lin, J.; Zhao, X.; Cui, Y.; Zhang, H.; Liao, D. Effect of Feedstock Solvent on the Stability of Cu/SiO₂ Catalyst for Vapor-Phase Hydrogenation of Dimethyl Oxalate to Ethylene Glycol. *Chem. Commun.* **2012**, *48*, 1177–1179. [[CrossRef](#)]
61. Van Der Grift, C.J.G.; Wielers, A.F.H.; Jogh, B.P.J.; Van Beunum, J.; De Boer, M.; Versluijs-Helder, M.; Geus, J.W. Effect of the Reduction Treatment on the Structure and Reactivity of Silica-Supported Copper Particles. *J. Catal.* **1991**, *131*, 178–189. [[CrossRef](#)]

Disclaimer/Publisher’s Note: The statements, opinions and data contained in all publications are solely those of the individual author(s) and contributor(s) and not of MDPI and/or the editor(s). MDPI and/or the editor(s) disclaim responsibility for any injury to people or property resulting from any ideas, methods, instructions or products referred to in the content.